Polymer Bulletin
https://doi.org/10.1007/s00289-019-02933-6

ORIGINAL PAPER

Suspension of poly(*o*-toluidine)-coated silica-based core–shell-structured composite in silicone oil: fabrication and rheological properties at different external electric field strengths

Quang-Vu Bach[1] · Cuong Manh Vu[2,3] · Huong Thi Vu[4] · Dinh Duc Nguyen[5]

Received: 22 November 2018 / Revised: 27 July 2019 / Accepted: 26 August 2019

Abstract

In this study, suspensions of core–shell particles dispersed in a silicone oil were fabricated and their rheological properties were evaluated at different external electric field strengths. The core–shell-structured composite materials were synthesized by coating poly(*o*-toluidine) (PoT) shells on the surfaces of silica particles. The silica particles were extracted from rice husk through acid and thermal treatments. The silica particles were then modified with (3-trimethoxysilyl)propyl methacrylate prior to the coating with the PoT shells. The chemical structures, morphologies, particle sizes, and elemental distributions of both silica and core–shell particles were investigated using scanning electron microscopy, Fourier-transform infrared spectroscopy, and energy-dispersive X-ray spectroscopy. Additionally, the rheological properties, chain formations, and dielectric properties of the suspensions were analyzed using rotational rheometry, optical microscopy, and an inductance–capacitance–resistance meter. The shear stress increased with the electric field strength along with the electro-rheological efficiency. The plot of the yield stress against the applied electric field strength exhibited a slope of 1.5. The fabricated core–shell particles are environment-friendly and are promising materials for applications in next-generation electro-rheological fluids.

Keywords Rice husk · Silanized silica · Electro-rheological fluid · Rheological properties · Silicone oil · Core–shell particle

✉ Cuong Manh Vu
vumanhcuong@duytan.edu.vn; vumanhcuong309@gmail.com

Extended author information available on the last page of the article

Published online: 28 August 2019

Introduction

Several smart materials with diverse rheological and mechanical properties have been fabricated with external stimuli such as electric and magnetic fields. These materials can be employed in various technological applications such as dampening, drug delivery, microfluidics, and robotics [1–3]. Among smart materials, electro-rheological (ER) fluids are notable owing to their phase changes between liquid- and solid-like states upon the application of an external electric field [4–9].

Generally, an ER fluid is a suspension of dielectric particles (dispersed phase) in a non-conducting liquid. Synthesized inorganic [10, 11], core–shell-structured composite [12], and hollow conductive polymer [13, 14] particles can be used as the dispersed phase. These phases polarize under an external electric field owing to the difference in dielectric constants between the particles and the medium. Consequently, chains are formed owing to the dipole–dipole interactions, which rapidly alter their rheological properties from liquid- to solid-like state. This behavior can be reversed in a very short time of only a few milliseconds [15]. This phenomenon was discovered by Winslow in 1949 and was characterized by the increase in viscosity of a colloidal suspension under an applied electric field [16]. Since the first report, this phenomenon has been extensively studied [17–19] owing to not only the various potential engineering applications but also scientific interest for these materials as one of the most exciting and complex soft materials [20–22]. Many types of electro-responsive material have been successfully used for the fabrication of ER fluids. However, core–shell particles have become the most promising materials for the fabrication of ER fluids, compared with pure polymer and pure inorganic materials, owing to the ease of controlling the particle shape, density, size, and electrical conductivity [23]. Polyaniline [24–32] and its derivatives [33–35] are also commonly used conductive polymers for the fabrication of ER fluids.

In recent years, biomaterials have been replacing synthesized materials as they offer several environmental advantages. Rice husk-based silica is considered valuable for the fabrication of composite materials. Rice husk is a relatively low-value agricultural by-product. Large quantities of rice husk are produced annually in agricultural countries and are generally burned or discarded, leading to negative environmental effects.

In this study, rice husk was utilized as a sustainable resource for the fabrication of bio-silica. The fabricated particles were employed as cores to produce core–shell particles coated with poly(*o*-toluidine) (PoT) shells. The methacryloxy group was also grafted onto the silica surface to increase the chemical affinity between the core and shell through π–π* interactions. Furthermore, the rheological properties of the ER fluid were analyzed in detail. The results suggest that fabricated core–shell particles could be used in automotive brakes. To the best of our knowledge, the use of PoT-coated silica in the fabrication of ER fluids has not been reported earlier, and we believe that this study will contribute to improving agricultural waste management and protecting the environment.

Experimental methods

Materials

Rice husks were collected from Huu Duc Food Commerce (Vietnam). H_2SO_4, silicone oil, and HCl (37%) were purchased from Xilong Scientific Co., Ltd. (China). (3-Trimethoxysilyl)propyl methacrylate, potassium persulfate (PPS) (≥ 99%), and *o*-toluidine (≥ 99%) were supplied by Sigma-Aldrich (Vietnam).

Preparation of the rice husk-based silica

The silica particles were prepared using a customized solution method followed by thermal evaporation. Initially, the collected rice husks were washed with distilled water to remove the dust and impurities. The washed rice husk was then dried in a laboratory oven until receiving the constant weight. Subsequently, 90 g of rice husks was blended in a 450-g solution of 4-wt% H_2SO_4 in distilled water and then stirred at 90 °C for 3 h to remove metal oxides and, thus, avoid the formation of black particles. The pretreated rice husk was then washed several times with deionized (DI) water to achieve a pH value of 7. The husks were then dried at 100 °C for 1 h before being calcinated in a muffle furnace at 800 °C for 7 h. The yield of silica was approximately 12 wt% of the rice husk.

Core–shell particle fabrication

First, 12 g of silica particles was immersed in a 150-mL solution of 1 M of HCl and stirred for 24 h, followed by washing with DI water and drying in a vacuum oven at 60 °C. The acid-pretreated silica particles were then stirred in a solution containing toluene (150 mL) and (3-trimethoxysilyl)propyl methacrylate (10 mL) for 2 days. The modified bio-silica particles were collected and washed with a solvent of toluene and ethanol (1:1 v/v) prior to being dried in the laboratory oven at 60 °C.

Second, the silanized silica particles (5 g) were thoroughly mixed in 280 mL of DI water, followed by the addition of 120 mL of a 1-M HCl solution. Subsequently, 1.26 g of *o*-toluidine and 3.75 g of PPS were simultaneously added to the above mixture. The solution was continuously stirred using a magnetic stirrer for 1 day. The core–shell particles were washed several times with ethanol and dried in a vacuum oven at 60 °C for 3 h. The procedure is illustrated in Fig. 1.

Preparation of the ER fluid

To prepare the ER fluid, the core–shell-structured particles were vigorously shaken in a silicone oil (approximately 20 vol. %). Sonication was used to obtain a fine suspension.

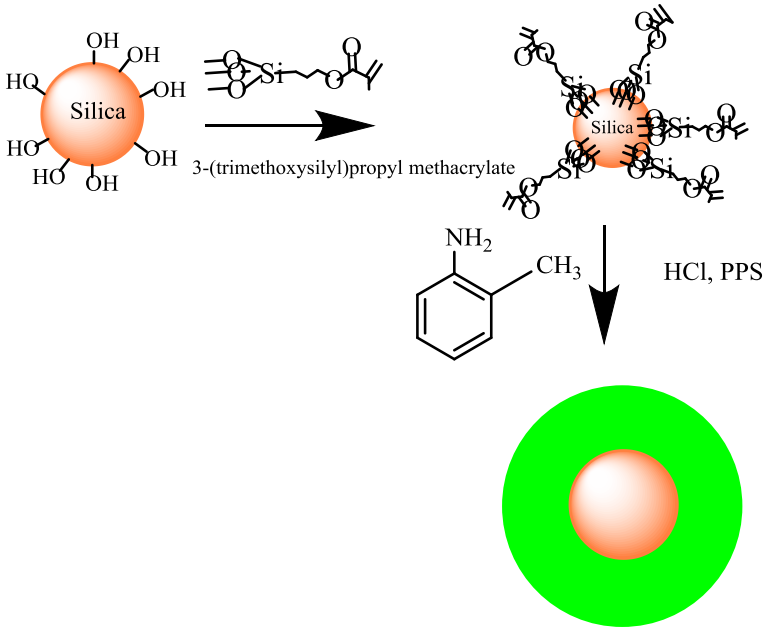

Fig. 1 PoT coating on the silica surface

Characterization

The surface morphologies, thermal properties, elemental distributions, and chemical structures of both SiO_2 and core–shell particles were analyzed using scanning electron microscopy (SEM, S-4300, Hitachi, Japan), thermogravimetric analysis (TGA, 4000 PerkinElmer) in air, energy-dispersive X-ray spectroscopy (EDS), and Fourier-transform infrared (FTIR) spectroscopy (Spectrum Two PerkinElmer), respectively. Transmission electron microscopy (TEM) was performed using a JEOL TEM 5410 NV system (Japan). The chain formation in the ER system under the applied electric field was observed by optical microscopy (Olympus BX51, USA). The electrical conductivity of the core–shell particle was 5.68×10^{-12} S cm^{-1}, measured using a resistivity meter (MCP-T610, Mitsubishi, Japan). A rotational rheometer (MCR 300, Physica, Stuttgart, Germany) equipped with a high-voltage supply was used to determine the rheological properties of the ER fluids. The dielectric properties of the ER fluids were investigated using an inductance–capacitance–resistance (LCR) meter (Agilent HP 4284A).

Results and discussion

Characterization of the core–shell particles

The morphologies of the silica and core–shell particles are presented in Fig. 2.

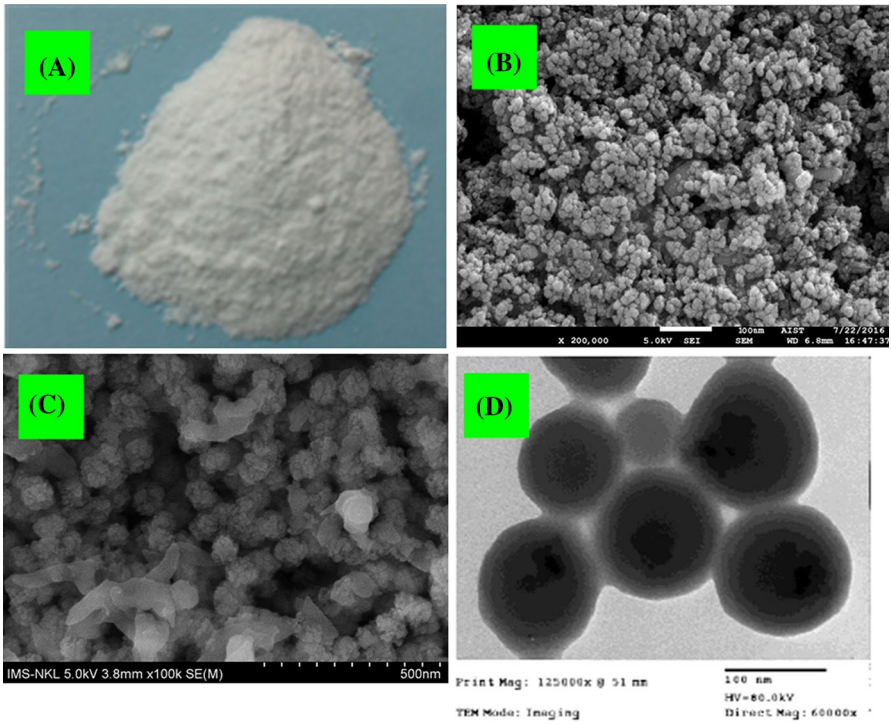

Fig. 2 **a** Image of the rice husk-based silica, SEM images of the **b** silica and **c** silica/PoT core–shell particles, and **d** TEM image of the silica/PoT core–shell particle

Figure 2 shows that both silica (Fig. 2b) and core–shell (Fig. 2c, d) particles have sizes in the range of 40–60 nm. The shell of the core–shell particle is shown in the TEM image in Fig. 2d.

The chemical structures and elemental distributions of the silica and core–shell particles were evaluated using FTIR spectroscopy and EDS, as shown in Figs. 3, 4, and 5.

Both silica (Fig. 3a) and silanized silica (Fig. 3b) exhibited three peaks at 1056, 800, and 443 cm^{-1} corresponding to the Si–O–Si bond. Compared with the FTIR spectrum of silica, that of the silanized silica (Fig. 3b) contains new peaks at 1640, 1720, 2950, and 2930 cm^{-1} corresponding to C=C, C=O, CH_3, and CH_2, respectively. This shows that the methacryloxy groups were successfully grafted onto the silica surface.

In the next step, the silanized silica particles were coated with PoT shells, as shown in Fig. 1. In this step, the PPS acted as an initiator, while the HCl helped convert the *o*-toluidine into an *o*-methyl phenyl ammonium ion. The o-methyl phenyl ammonium ions were then polymerized into PoT by an oxidation reaction of the PPS.

The FTIR spectrum of the core–shell particle (Fig. 4b) shows new peaks at 1560, 1481, 3422, 2963, and 1292 cm^{-1} assigned to C=N, C=C, N–H, C–H, and C–N stretching vibrations, respectively, compared with the FTIR spectrum of the silica

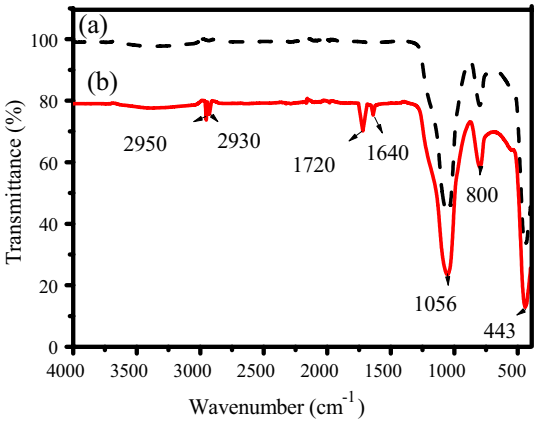

Fig. 3 FTIR spectra of the **a** rice husk-based silica and **b** silica treated with 3-(trimethoxysilyl) propyl methacrylate

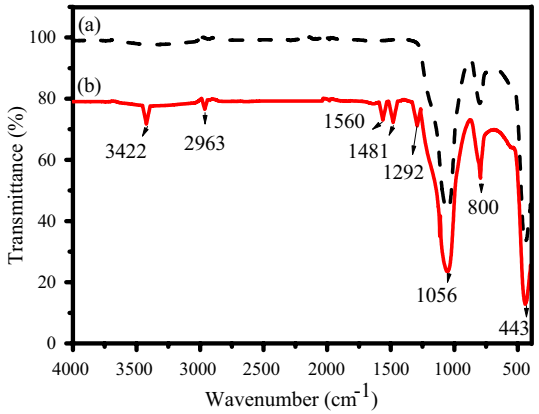

Fig. 4 FTIR spectra of the **a** rice husk-based silica and **b** bio-silica/PoT core–shell-structured particles

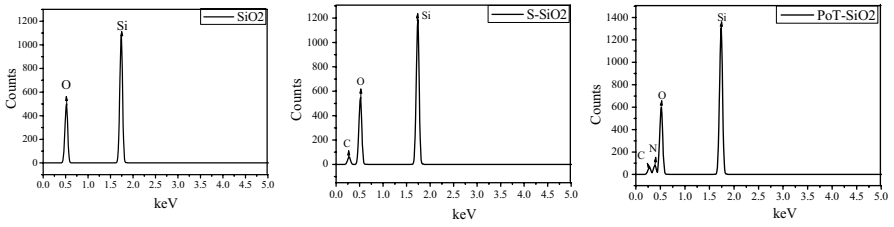

Fig. 5 ED spectra of SiO_2, silanized SiO_2 (S-SiO_2), and PoT–SiO_2 core–shell particles

particle. The peaks at 800 and 443 cm^{-1} are the major peaks of the silica Si–O–Si stretching vibrations. The Si–O–Si antisymmetric stretching and Si–OH bending exhibited a peak at 1056 cm^{-1}.

The ED spectra confirmed the successful silanization processing and formation of core–shell particles, in agreement with the FTIR spectra. The ED spectrum of silica (Fig. 5a) shows only two peaks of Si and O, while that of the silanized

silica (Fig. 5b) shows a new peak of C. The ED spectrum of the core–shell particle (Fig. 5c) shows new peaks of C and N atoms. In addition, the peak intensities of Si and O of the silanized silica and core–shell particles are increased compared with those of pristine silica.

TGA was used to determine the thermal stabilities of the silica and core–shell particles, as shown in Fig. 6.

Weight loss of silica (Fig. 6a) was observed around 300 °C, which occurred owing to the decomposition of oxygen functional groups on the silica surface. Notably, no weight loss was observed below 300 °C, which suggests the presence of moisture on the silica surface. The first weight loss of the core–shell particle (Fig. 6b) was observed around 150 °C, owing to the removal of the moisture. The fraction of PoT shell was 8 wt%, obtained by the different weight losses of the silica and core–shell particles at 800 °C.

The fabricated core–shell particles were used as the dispersed phase in the preparation of the ER fluid. One of the most important characteristics of the ER fluid, the formation of a chain under the electric field, was observed using optical microscopy. The ER fluid based on the silica/PoT core–shell particles was placed between two electrodes.

Figure 7 shows that the particles were freely dispersed in the absence of an electric field (Fig. 7a). In contrast, chains were formed when an electric field was applied (Fig. 7b).

The changes in shear stress of the ER fluid as a function of the shear rate at different external electric field strengths were evaluated, as shown in Fig. 8a. The ER fluid exhibited the Newtonian behavior in the absence of the external electric field. In the presence of the electric field, the ER fluid exhibited a non-Newtonian behavior owing to the polarization and formed a chain structure. The yield stress increased with the electric field strength. At all applied electric field strengths, the ER fluid plateaued with a constant shear stress at low shear rates because of the balance between the hydrodynamic breaking force and electrostatic interaction induced by the changing electric field. The Bingham fluid model was employed to fit the flow curves in Fig. 8a:

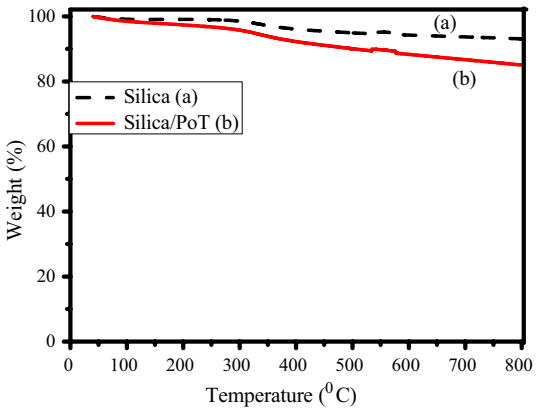

Fig. 6 TGA of the **a** bio-silica and **b** bio-silica/PoT core–shell particles

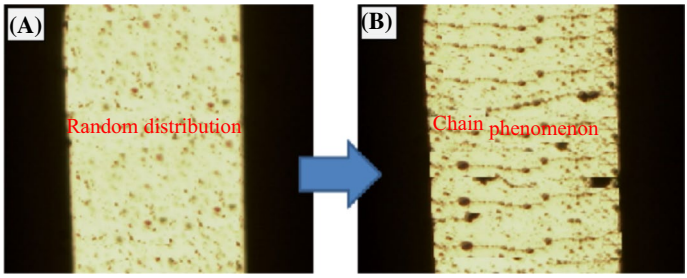

Fig. 7 Optical microscopy image of the bio-silica/PoT core–shell microsphere: **a** 0 and **b** 300 V

$$\tau = \tau_y + \eta\dot{y}, \quad \tau \geq \tau_y \tag{1}$$

$$\dot{\gamma} = 0, \quad \tau < \tau_y.$$

The Bingham's equation contains two basic parameters, Newtonian viscosity η and yield stress τ_y. The values of these parameters are presented in Table 1.

Figure 8b presents the relations between the shear viscosity and shear rate of the silica/PoT-based ER fluid at different external electric field strengths. In the absence of electric field, the ER fluid exhibited a slight deviation from the Newtonian behavior in the low shear rate region, while in the high shear rate region, it exhibited the Newtonian fluid characteristic with a constant shear viscosity. In the presence of the external electric field, the shear thinning phenomenon with the decrease in shear viscosity could be observed with the increase in shear rate. The zero-shear viscosity also increased with the electric field strength. The shear thinning phenomenon indicates that the bio-silica/PoT particles in the ER fluid were initially linked with the chain under the external electric field and then broke down by the shear flow. The same trend was also reported by Wang et al. [14]. However, the shear stress and shear viscosity in this study seem to be higher at the same electric field strength.

The ER efficiency is considered one of the important characteristics of the ER fluid. The ER efficiency can be used to evaluate the change in ER system in the presence of an electric field. The ER efficiency was calculated by

$$e = \frac{(\eta_E - \eta_0)}{\eta_0}, \tag{2}$$

where η_E and η_0 are the viscosities in the presence and absence of the external electric field, respectively. The change in ER efficiency as a function of the shear rate is presented in Fig. 8c. The ER efficiency increased with the electric field strength.

The viscoelastic properties of the ER fluid were investigated by an oscillation test to evaluate the linear viscoelastic region in the strain amplitude sweep at a fixed angular frequency of 6.28 rad s^{-1}. Figure 9 shows the relations between the storage and loss moduli and strain at different electric field strengths for the bio-silica/PoT-based ER fluid. The storage modulus (G') is related to the elastic properties, while the loss modulus is an indicator of the viscous properties. As shown in Fig. 9, all storage moduli were higher than the loss moduli. This implies

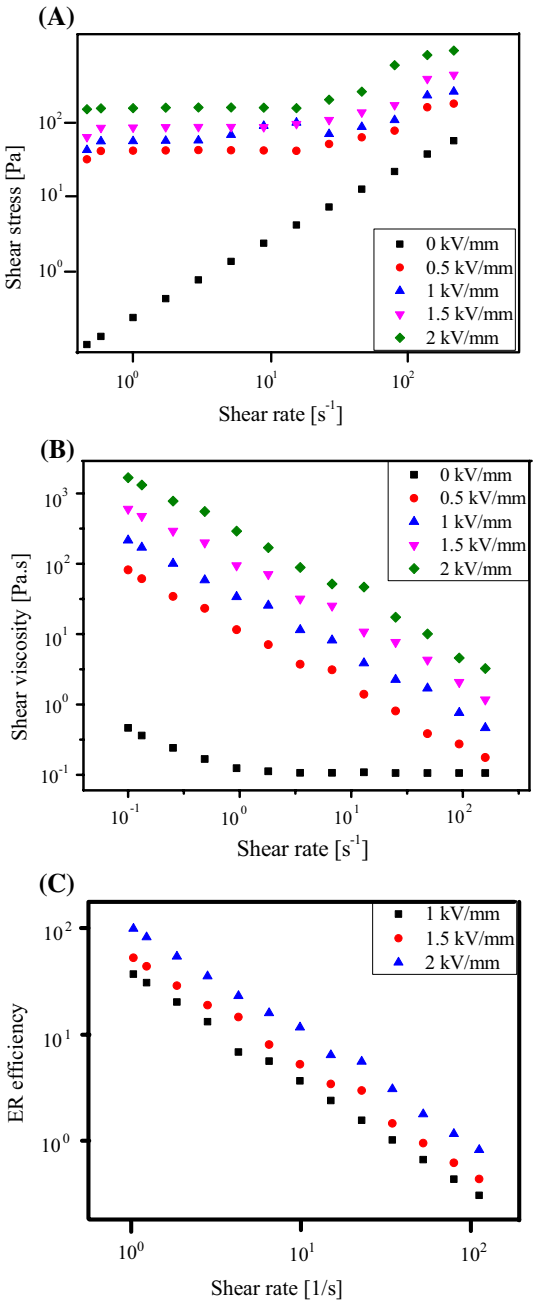

Fig. 8 **a** Shear stress, **b** viscosity, and **c** ER efficiency of the 20-vol% silica/PoT ER fluid as functions of the shear rate at different electric field strengths

that the elastic rather than the viscous properties are predominant owing to the chain formation in the ER fluid under the applied electric field, leading to the transfer from the liquid- to the solid-like state. The critical strain in the plateau

Table 1 Bingham model parameters of the silica/PoT-based ER fluid

ER fluid	Parameter	0.5 kV/mm	1 kV/mm	1.5 kV/mm	2 kV/mm
Silica/PoT	τ_0	16.8	29.34	61	102
	η_0	0.102	0.132	0.18	0.245

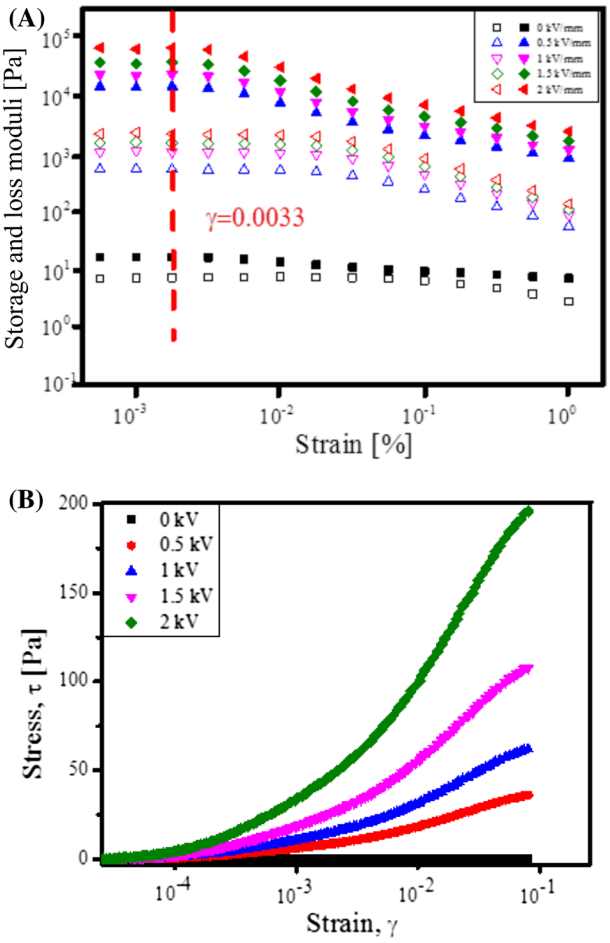

Fig. 9 **a** Storage modulus, loss modulus, and **b** elastic stress as functions of the strain

region was 0.0033 for the frequency sweep. The relationship between the elastic stress and strain is shown in Fig. 9. The maxima of the elastic stress provide a quantitative approach to localize the shear yield points. In the absence of electric field, the elastic strength was zero, while elastic strength emerged at all electric field strengths owing to the chain formation in the ER fluid. The elastic strength

increased with the electric field strength, which implies that the force between the particles in the chain was larger at a higher electric field strength.

Figure 10 shows the dynamic and elastic yield stresses as functions of the electric field strength. The dynamic yield stress was obtained by controlled shear rate tests using a shear stress extrapolation at the extremely low shear rate limit (Fig. 8a). On the other hand, the elastic yield stress was deduced from dynamic oscillation measurements with a strain amplitude sweep test (Fig. 9b). The elastic yield stress was higher than the dynamic yield stress. These results are in agreement with those in other reports [34, 35].

The dielectric properties are also considered important characteristics of the ER fluid and are related to the speed of interfacial polarization. In this study, the dielectric properties were evaluated using an LCR meter. Figure 11a, b presents the dielectric constant and dielectric loss as functions of the frequency (ω) and Cole–Cole plot of the bio-silica/PoT-based ER fluid, respectively. The dielectric constant decreased with the increase in frequency, while the dielectric loss had the maximum value at a specific frequency. The Cole–Cole equation can be expressed as

$$\varepsilon^* = \varepsilon' - i\varepsilon'' = \varepsilon_\infty + \frac{\varepsilon_0 - \varepsilon_\infty}{1 + (i\omega\lambda)^{(1-\alpha)}}, \quad 0 \le \alpha \le 1, \tag{3}$$

where ε_0 is ε' at $\omega \to 0$, ε_∞ is ε' at $\omega \to \infty$, λ is the relaxation time of the interfacial polarization, and $\Delta\varepsilon = \varepsilon_0 - \varepsilon_\infty$ indicates the achievable polarizability of the particles in the ER fluid. The exponent $(1-\alpha)$, indicates the broadness of the relaxation time distribution.

Table 2 shows the fitting parameters of the Cole–Cole equation. The core–shell particles were quickly polarized under the applied electric field.

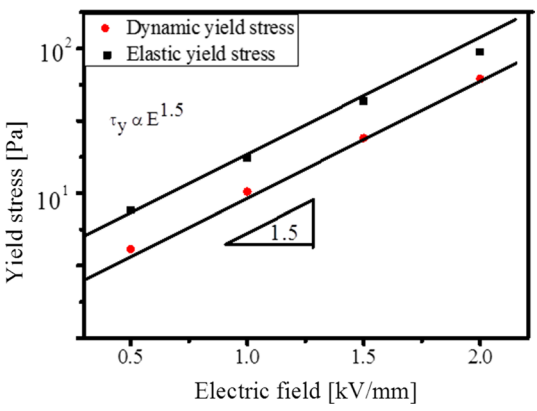

Fig. 10 Yield stress as a function of the electric field

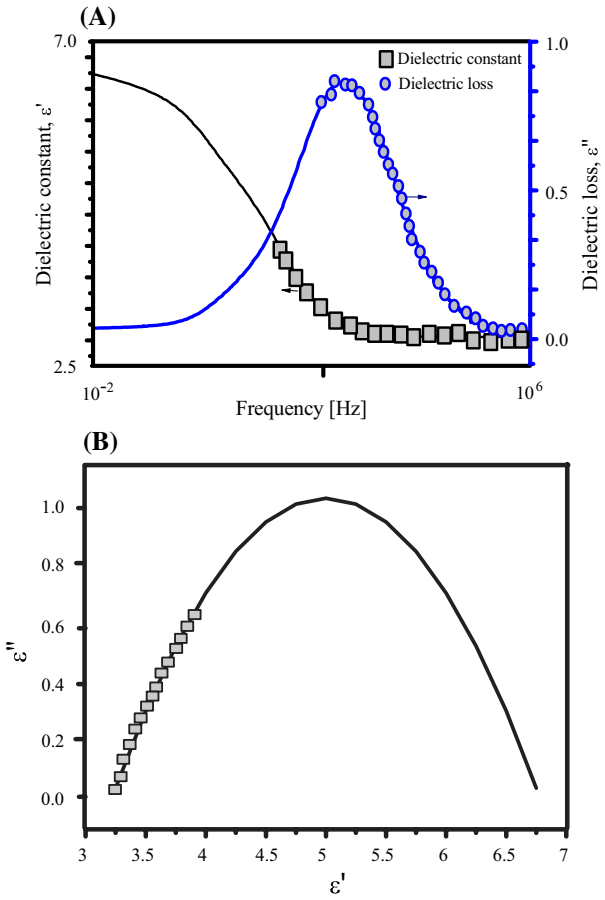

Fig. 11 Dielectric properties of the ER fluid

Table 2 Dielectric characteristics [Eq. (3)]

Parameter	ε_0	ε_∞	$\Delta\varepsilon=\varepsilon_0-\varepsilon_\infty$	λ	$1-\alpha$
Value	6.68	2.6	4.08	0.016	0.62

Conclusions

Silica nanoparticles were extracted from rice husks using a simple method that combined acid and thermal treatments. The surface of the bio-silica was modified with 3-(trimethoxysilyl)propyl methacrylate to activate the methacryloxy group. The bio-silica/PoT core–shell particles were synthesized by chemical oxidative polymerization and characterized using TEM, FTIR spectroscopy, EDS, and TGA. The rheological test indicated that the shear stress fitted the Bingham model. In addition, the storage modulus was higher than the loss modulus, while the ER efficiency increased with

the electric field strength. The dielectric properties of the ER fluid were correlated with the Cole–Cole equation. The dielectric constant decreased with the increase in frequency, while the dielectric loss had the maximum value at the specific frequency.

Funding This research was funded by the Vietnam National Foundation for Science and Technology Development (NAFOSTED) under grant number 104.02-2017.15.

References

1. Yin J, Wang X, Chang R, Zhao X (2012) Polyaniline decorated graphene sheet suspension with enhanced electrorheology. Soft Matter 8:294–297
2. Shin K, Kim D, Cho JC, Lim HS, Kim JW, Suh KD (2012) Monodisperse conducting colloidal dipoles with symmetric dimer structure for enhancing electrorheology properties. J Colloid Interface Sci 374:18–24
3. Gong X, Wang L, Wen W (2009) Design and fabrication of monodisperse hollow titania microspheres from a microfluidic droplet-template. Chem Commun 31:4690–4692
4. Sedlacik M, Mrlik M, Kozakova Z, Pavlinek V, Kuritka I (2013) Synthesis and electrorheology of rod-like titanium oxide particles prepared via microwave-assisted molten-salt method. Colloid Polym Sci 291:1105–1111
5. Wang B, Yin Y, Liu C, Yu S, Chen K (2013) Synthesis of flower-like BaTiO3/Fe3O4 hierarchically structured particles and their electrorheological and magnetic properties. Dalton Trans 42:10042–10055
6. Cheng Y, Guo J, Liu X, Sun A, Xu G, Cui P (2011) Preparation of uniform titania microspheres with good electrorheological performance and their size effect. J Mater Chem 21:5051–5056
7. Wu J, Jin T, Liu F, Guo J, Cheng Y, Xu G (2014) Formamide-modified titanium oxide nanoparticles with high electrorheological activity. RSC Adv 4:29622–29628
8. Tang J, Wen X, Liu Z, Wang J, Zhang P (2018) Synthesis and electrorheological performances of 2D PANI/TiO2 nanosheets. Colloids Surf A Physicochem Eng Asp 552:24–31
9. Xinrong S, Aiqing H, Nianyuan T, Dan M, Yuanbin L (2011) Influence of amphiprotic groups on the electrorheological behavior of polymers. Mater Chem Phys 126:369–374
10. He K, Wen Q, Wang C, Wang B, Yu S, Hao C, Chen K (2017) Synthesis of anatase TiO_2 with exposed (100) facets and enhanced electrorheological activity. Soft Matter 13:7879–7889
11. He K, Wen Q, Wang C, Wang B, Yu S, Hao C, Chen K (2017) The preparation and electrorheological behavior of bowl-like titanium oxide nanoparticles. Soft Matter 13:7677–7688
12. Liu W, Xie Z, Lu Y, Gao M, Zhang W, Gao L (2019) Fabrication and excellent electroresponsive properties of ideal PMMA@$BaTiO_3$ composite particles. RSC Adv 9:12404–12414
13. Sung BH, Ko YG, Choi US (2007) Novel synthesis and electrorheological properties of monodispersed submicron-sized hollow polyaniline dicarboxylate salt form suspensions. Colloids Surf A Physicochem Eng Asp 292:217–223
14. Wang B, Tian X, He K, Ma L, Yu S, Hao C, Chen K, Lei Q (2016) Hollow PAQR nanostructure and its smart electrorheological activity. Polymer 83:129–137
15. Tilki T, Yavuz M, Karabacak C, Cabuk M, Ulutürk M (2010) Investigation of electrorheological properties of biodegradable modified cellulose/corn oil suspensions. Carbohydr Res 345:672–679
16. Winslow WM (1949) Induced fibration of suspensions. J Appl Phys 20:1137
17. Zukoski CF (1993) Material properties and the electrorheological response. Annu Rev Mater Sci 23:45–78
18. Block H, Kelly JP (1988) Electro-rheology. J Phys D Appl Phys 21:1661
19. Hao T (2001) Electrorheological fluids. Adv Mater 13:1847–1857
20. Hao T, Kawai A, Ikazaki F (1998) Mechanism of the electrorheological effect: evidence from the conductive, dielectric, and surface characteristics of water-free electrorheological fluids. Langmuir 14:1256–1262
21. Yethiraj A (2007) Tunable colloids: control of colloidal phase transitions with tunable interactions. Soft Matter 3:1099–1115

22. Stokes JR, Frith WJ (2008) Rheology of gelling and yielding soft matter systems. Soft Matter 4:1133–1140
23. Yilmaz H, Unal HI, Sari B (2007) Synthesis, characterization and electrorheological properties of poly(*o*-toluidine)/Zn conducting composites. J Appl Polym Sci 103:1058–1065
24. Zhou Y, Qin ZY, Li L, Zhang Y, Wei YL, Wang LF, Zhu MF (2010) Polyaniline/multi-walled carbon nanotube composites with core–shell structures as supercapacitor electrode materials. Electrochim Acta 55:3904–3908
25. Ozkan S, Unal HI, Yılmaz E, Suludere Z (2015) Electrokinetic and antibacterial properties of needle like TiO_2/polyrhodanine core/shell hybrid nanostructures. J Appl Polym Sci 132:41554
26. Yeh JM, Kuo TH, Huang HJ, Chang KC, Chang MY, Yang JC (2007) Preparation and characterization of poly(*o*-methoxyaniline)/Na^+–MMT clay nanocomposite via emulsion polymerization: electrochemical studies of corrosion protection. Eur Polym J 43:1624–1634
27. Dey A, De S, De A, De SK (2004) Characterization and dielectric properties of polyaniline–TiO2 nanocomposites. Nanotechnology 15:1277–1283
28. Wen Q, He K, Wang C, Wang B, Yu S, Hao C, Chen K (2018) Clip-like polyaniline nanofibers synthesized by an insitu chemical oxidative polymerization and its strong electrorheological behavior. Synth Met 239:1–12
29. Wen Q, Ma L, Wang C, Wang B, Han R, Hao C, Chen K (2019) Preparation of core–shell structured metal–organic framework@PANI nanocomposite and its electrorheological properties. RSC Adv 9:14520–14530
30. Tang J, Wen X, Liu Z, Wang J, Zhang P (2018) Synthesis and electrorheological performances of 2D PANI/TiO_2 nanosheets. Colloid Surf A: Physicochem Eng Asp 552:24–31
31. Yin J, Zhao X, Xia X, Xiang L, Qiao Y (2008) Electrorheological fluids based on nano-fibrous polyaniline. Polymer 49:4413–4419
32. Gercek B, Yavuz M, Yilmaz H, Sari B, Unala HI (2007) Comparison of electrorheological properties of some polyaniline derivatives. Colloids Surf A Physicochem Eng Asp 299:124–132
33. Huiru MA, Jianguo G, Runzhang Y (2005) Electrorheological properties of suspensions of PAn–PEO–PAn triblock copolymer particles. J Wuhan Univ Technol Mater Sci Ed 20:43–45
34. Zhang L, Su K, Li X (2003) Electrorheological effects of polyaniline-type electrorheological fluids. J Appl Polym Sci 87:733–740
35. Liu J, Wen X, Liu Z, Tan Y, Yang S, Zhang P (2015) Electrorheological performances of poly(*o*-toluidine) and *p*-toluenesulfonic acid doped poly(*o*-toluidine) suspensions. Colloid Polym Sci 293:1391–1400

Affiliations

Quang-Vu Bach[1] · Cuong Manh Vu[2,3] · Huong Thi Vu[4] · Dinh Duc Nguyen[5]

Quang-Vu Bach
bachquangvu@tdtu.edu.vn

[1] Sustainable Management of Natural Resources and Environment Research Group, Faculty of Environment and Labour Safety, Ton Duc Thang University, Ho Chi Minh City, Vietnam

[2] Center for Advanced Chemistry, Institute of Research and Development, Duy Tan University, Da Nang, Vietnam

[3] Faculty of Chemical-Physical Engineering, Le Qui Don Technical University, 236 Hoang Quoc Viet, Hanoi, Vietnam

[4] AQP Research and Control Pharmaceuticals Joint Stock Company (AQP Pharma J.S.C) Dong Da, Hanoi, Vietnam

[5] Department of Environmental Energy and Engineering, Kyonggi University, Suwon 442-760, Korea